Journal of Biomolecular NMR **30:** 195–204, 2004.
© 2004 *Kluwer Academic Publishers. Printed in the Netherlands.*

An on/off resonance rotating frame relaxation experiment to monitor millisecond to microsecond timescale dynamics

Seho Kim & Jean Baum*
Department of Chemistry and Chemical Biology, Rutgers University, Piscataway, NJ 08854, U.S.A.

Received 10 February 2004; Accepted 10 June 2004

Key words: adiabatic pulses, heteronuclear relaxation, $R_{1\rho}$ experiment, protein dynamics

Abstract

Rotating frame relaxation experiments in proteins are used to study slow motions on the microsecond to millisecond timescale. An on/off resonance rotating frame relaxation experiment ($R_{1\rho}$) has been developed that incorporates adiabatic rotations into a $R_{1\rho}$–R_1 constant relaxation time experiment with weak radio frequency field strengths in order to effectively lock the magnetization over a wide range of ^{15}N frequencies. The new pulse sequence allows the measurement of a wide range of chemical exchange timescales on the order of 1.0 to 0.05 ms over an asymmetric bandwidth from $+1.7\omega_1$ to $-0.5\omega_1$ in a single experiment. A total bandwidth of $\pm 1.7\omega_1$ is obtained by performing the experiment a second time with a reversed adiabatic rotation.

Introduction

NMR plays a central role in determining the dynamics of proteins by providing experiments that allow a detailed description of the amplitudes and kinetic rate constants of motions on the μs and ms timescales. ^{15}N and ^{13}C relaxation experiments have been developed to measure backbone and side-chain conformational motions and have been used to study the relationship between dynamics and structure, function, and folding (Frauenfelder et al., 1991; Palmer et al., 1996; Palmer, 1997, 2001; Kay, 1998).

A number of ^{15}N relaxation experiments have been proposed to measure chemical exchange processes on the μs-ms timescale. The R_2^{cpmg} (transverse relaxation rate, R_2, using Carr–Purcell–Meiboom–Gill pulses) (Carver and Richards, 1972; Orekhov et al., 1994) and $R_2^{rc\text{-}cpmg}$ (relaxation-compensated CPMG) (Loria et al., 1999; Wang et al., 2001) experiment rely on the delay between pulses in the spin-echo pulse train and the on- and off-resonance $R_{1\rho}$ (rotating frame relaxation rate) experiments (Szyperski et al., 1993; Akke and Palmer, 1996; Zinn-Justin et al., 1997; Mulder et al., 1998; Massi et al., 2004) rely on the presence of a continuously applied radio frequency (rf) field to determine the exchange contribution to relaxation. The contribution of chemical exchange (R_{ex}) to $R_{1\rho}$ in the presence of a continuous spin-lock has been formulated under on- and off-resonance conditions and is given by Deverell et al. (1970); Davis et al. (1994); Trott and Palmer (2002):

$$R_{1\rho} - R_1 = (R_2 - R_1 + R_{ex}) \sin^2 \theta, \tag{1}$$

$$R_{ex} = P_A P_B (\delta\omega)^2 \tau_{ex} / (1 + \tau_{ex}^2 \omega_e^2), \tag{2}$$

where $R_{1\rho}$ is a weighted sum of the longitudinal relaxation rate (R_1) and the transverse relaxation rate (R_2), $\delta\omega$ is the frequency difference of two exchanging states A and B with populations P_A and P_B, and τ_{ex} is the chemical exchange timescale. ω_e is the effective spin-lock field strength given by $(\omega_1^2 + \Omega^2)^{1/2}$ where Ω is the resonance offset from the carrier frequency, ω_1 is the applied rf spin-lock field strength and θ is the tilt angle defined as $\arctan(\omega_1/\Omega)$.

The dependence of the chemical exchange term R_{ex}, on the effective field strength, ω_e, and the chemical exchange timescale τ_{ex} is plotted in Figure 1. As the chemical exchange timescale, τ_{ex}, becomes slower, the ω_e field dependence of R_{ex} becomes more

*To whom correspondence should be addressed. E-mail: baum@rutchem.rutgers.edu

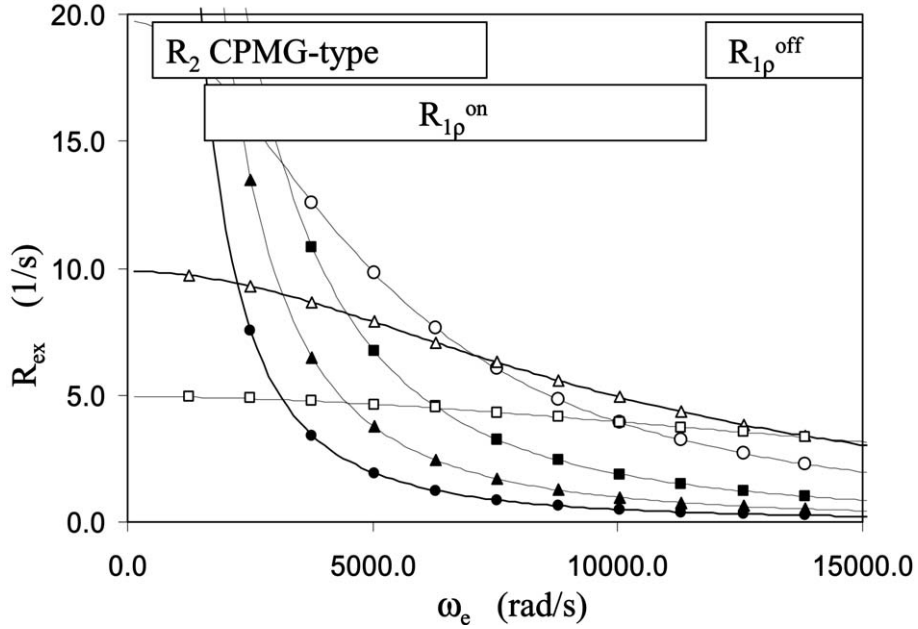

Figure 1. Chemical exchange contribution (R_{ex}) as a function of effective field strength, ω_e (Equation (2)) for two site conformational exchange with $\delta\omega = 628.3$ rad/s, and exchange timescales of 2.0(●), 1.0(▲), 0.5(■), 0.2(○), 0.1(△), and 0.05(□) ms. The range of effective field strengths (ω_e) over which different relaxation experiments can be applied, are shown in the boxes. For R_2^{cpmg} experiments, the practical range of field strengths is 1570–7850 rad/s when inter-pulse delays (τ_{cp}) in the CPMG sequence are 1.0–0.2 ms and ω_e is equated with $\pi/2\tau_{cp}$ (Orekhov et al., 1994). For $R_2^{rc\text{-}cpmg}$ (Loria et al., 1999; Wang et al., 2001), the range of ω_e is approximately 157–3140 rad/s as τ_{cp} can be as high as 10 ms. The combined range of CPMG-type relaxation experiments are shown as 157–7850 rad/s. In the off-resonance $R_{1\rho}$ ($R_{1\rho}^{off}$) experiments (Akke and Palmer, 1996; Zinn-Justin et al., 1997), the maximum strength is over 20000 rad/sec but the minimum strength is limited to about 12000 rad/s in order to meet the off-resonance condition. In the on-resonance $R_{1\rho}$ ($R_{1\rho}^{on}$) experiments (Szyperski et al., 1993; Massi et al., 2004), the maximum rf field strength is limited to about 2000 Hz due to probe heating and the reported minimum strength is 150 Hz. Spectral bandwidths are limited to within $\pm 0.4\omega_1$ corresponding to a minimum tilt angle of 68°. For the on- and off- resonance $R_{1\rho}$ ($R_{1\rho}^{on/off}$) experiment proposed here, weak effective fields are used with adiabatic rotations in order to increase the spectral bandwidth.

pronounced, especially at weaker fields. Thus, the range of chemical exchange timescales that can be measured by a particular relaxation experiment are determined by the window of effective field strengths that are accessible to that experiment. The range of effective field strengths, ω_e, that different relaxation experiments cover is mapped onto Figure 1. The off-resonance $R_{1\rho}$ ($R_{1\rho}^{off}$) experiment is practical at high field strengths beyond 12000 rad/s (Akke and Palmer, 1996; Akke et al., 1998), The R_2 CPMG-type experiments such as R_2^{cpmg} and $R_2^{rc\text{-}cpmg}$ experiments can be mapped onto weaker fields covering a range of 150 to 7850 rad/s (Orekhov et al., 1994; Loria et al., 1999; Wang et al., 2001) (see Figure 1 caption for details). As shown in Figure 1, slow chemical exchange timescales on the order of 1 to 10 ms can be obtained by measuring relaxation rates at weak fields with the R_2 CPMG-type experiments and faster exchange rates on the order of 0.2 ms to 25 μs are obtained by measuring relaxation rates at stronger fields with $R_{1\rho}^{off}$ experiments. In order to bridge the gap between the slow and fast chemical exchange timescales accessible by R_2 CPMG-type and $R_{1\rho}^{off}$ experiments, combined data analysis from separate R_2^{cpmg} and $R_{1\rho}^{off}$ experiments (Mulder et al., 1999) or on-resonance rotating frame relaxation experiments ($R_{1\rho}^{on}$) using weak radio frequency spin-lock field strengths (Szyperski et al., 1993; Massi et al., 2004) have been developed. These $R_{1\rho}^{on}$ experiments using weak rf field strengths allow a more complete characterization of the relaxation dispersion curves than could be sampled by conventional on- or off-resonance experiments using strong rf field strengths or by the CPMG experiment. However, these experiments are only accurate for spectral regions of $\pm 0.4\omega_1$ thereby limiting the range of ^{15}N frequencies that can be measured in a single experiment.

This paper describes $R_{1\rho}$ experiments that use near resonance conditions and weak rf field strengths while increasing the range of ^{15}N frequencies that can be

measured to $+1.7\omega_1$ to $-0.5\omega_1$ in a single experiment. This experiment covers the full range of ^{15}N frequencies in the spectrum even at weak rf fields corresponding to approximately 300 Hz. As described above, one problem encountered with the use of weak rf spin-lock field strengths is the difficulty of locking the magnetization along the effective field across the entire ^{15}N spectral width. Frequency and amplitude modulated adiabatic pulses have been proposed previously for use in off-resonance $R_{1\rho}$ experiments in order to improve the alignment of the magnetization with the off-resonance spin-lock field for large chemical shift dispersion (Mulder et al., 1998; Garwood and Ke, 1991; Ugurbil et al., 1988). Here, amplitude and phase modulated pulses are used with weak fields under near resonance conditions to spin-lock the magnetization at specific tilt angles across a wide range of ^{15}N chemical shifts. Near resonance conditions are maintained by locating the carrier position of the spin-lock pulses within the ^{15}N spectral widths. This allows relatively large tilt angles (from 90° to 30°) to be obtained even with the use of weak rf fields thereby optimizing sensitivity by measuring a large effect of R_{ex} on $R_{1\rho}$.

Materials and methods

The pulse sequence for the on/off resonance $R_{1\rho}$ ($R_{1\rho}^{on/off}$) experiment (Figure 2) is an extension of the $R_{1\rho}$-R_1 CRT (constant relaxation time) experiment (Akke and Palmer, 1996), incorporates adiabatic pulses with frequency and amplitude modulation (Mulder et al., 1998; Garwood and Ke, 1991; Ugurbil et al., 1988) and uses new decoupling schemes developed by Korzhnev al. (2002). Figure 2 shows that following the initial refocused INEPT the transverse ^{15}N magnetization is returned to the z-axis for the R_1 and $R_{1\rho}$ relaxation. During the delay T-t_{rel}, the longitudinal ^{15}N magnetization decays with the laboratory frame R_1 relaxation rate. At the end of the R_1 relaxation delay, rotation of ^{15}N magnetization by an adiabatic pulse (SP1) is performed to prepare the spin-lock at various tilt angles. The adiabatic pulse that is incorporated into the pulse sequence is an adiabatic half passage pulse (AHP) with frequency and amplitude modulation (Mulder et al., 1998; Garwood and Ke, 1991; Ugurbil et al., 1988). The amplitude, phase and frequency modulation of the AHP are shown in Figure S1 (Supplementary Material). During the delay t_{rel}, the tilted ^{15}N magnetization undergoes rotating frame $R_{1\rho}$ relaxation and is then brought back to the z-axis by a time-reversed adiabatic pulse, SP2. ^{1}H decoupling pulses during t_{rel} are used to suppress the effects of cross correlation between dipole-dipole and chemical shift anisotropy relaxation mechanisms. The decoupling scheme employs ^{1}H continuous wave irradiation where the phase is alternated between x and $-$x every 10 ms ($4\tau_b$) (Korzhnev et al., 2002). The pulse sequence provides the $R_{1\rho}$-R_1 relaxation rate during CRT by measuring intensity changes as a function of t_{rel}.

The $R_{1\rho}^{on/off}$ experiments are performed on a *de novo* four helix bundle protein S-824 containing 102 amino acid residues (Wei et al., 2003a, 2003b). The protein is designed from a focused combinatorial library with a binary pattern of polar and non-polar amino acids. The experimental ω_1 field strength and the rf carrier frequency of the AHP are simultaneously varied resulting in a range of tilt angles for each individual resonance. The combination of (ω_1, Ω') in Hz that are used in the $R_{1\rho}$ experiment are (1496, 0.0), (1082, 100.0), (1082, $-$100.0), (785, 200.0), (785, $-$200.0), (581, 300.0), (581, $-$300), (440, 400.0), (440, $-$400), (386, 500.0), (386, $-$500), (275, 500.0), and (275, $-$500) where Ω' is the difference between the carrier frequency for the AHP and spin-lock, and the carrier frequency at 117.53 ppm for the HSQC as shown in Figure 2. The resonance offset, Ω, is calculated by subtracting Ω' from each resonance frequency. For example, for residue N18 at 115.46 ppm, ω_e values are 9423, 6919, 6799, 5292, 4969, 4449, 3851, 4210, 3334, 4509, 3474, 4174, and 3027 rad/s with the experimental array indicated above and nominal tilt angles are 86.0, 79.2, 89.7, 68.8, 83.0, 55.1, 71.4, 41.1, 56.1, 32.5, 44.3, 24.4, and 34.9°. The ^{15}N spin-lock field strenghts were calibrated using the method of Guenneugues et al. (1999). The calibration strip plot and error ranges indicate that the field strengths are accurate to within 3% (Figure S2, Supplementary Material). For negative Ω', AHP with reversed frequency modulation was used to achieve uniform adiabatic rotations during SP1 and SP2. The tanh/tan adiabatic pulses have a duration of 4 ms and the spin-lock length is t_{rel}. To measure $R_{1\rho} - R_1$, 8 different relaxation delays (t_{rel} = 20, 40, 60, 90, 120, 150, 200, 250 ms) were used with T = 250 ms at each combined array of ω_1 and Ω'. ^{1}H-^{15}N HSQC spectra (Bax et al., 1990) with interleaved t_{rel} were collected on a Varian Inova 500 MHz NMR at 25 °C. The acquired 2D data of 1024 (t_2) × 240 (t_1) complex points were processed to a spectrum of 1024 × 256 real points with nmr-

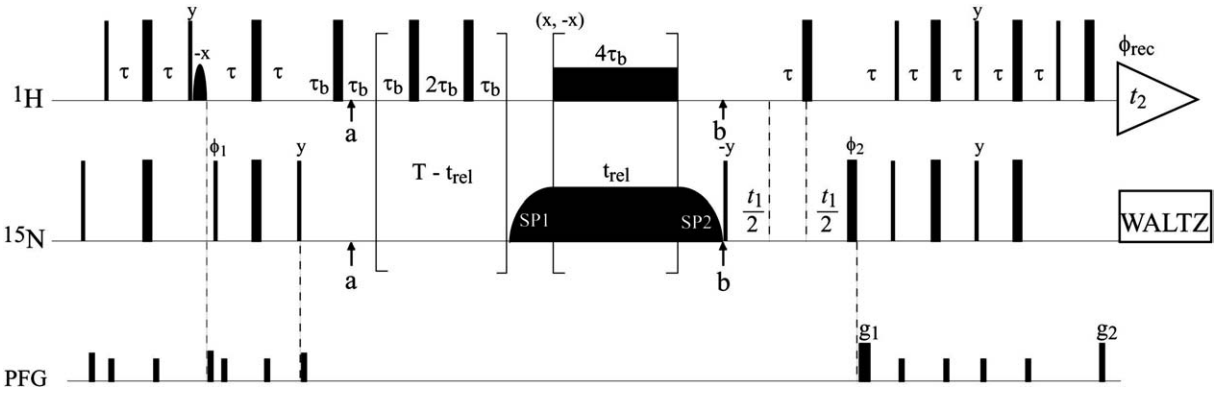

Figure 2. Pulse sequence for measurement of ^{15}N $R_{1\rho}^{on/off}$. The pulse sequence is a sensitivity-enhanced ^{1}H -^{15}N HSQC with refocused INEPT (Varian Protein Pack, gNHSQC) modified to include $R_{1\rho}$–R_1 constant relaxation scheme with adiabatic rotations. Delays are $\tau = 2.5$ ms and $\tau_b = 2.5$ ms. Phase cycles are $\phi_1 = 4(x,-x)$; $\phi_2 = x,x,y,y,-x,-x,-y,-y$; $\phi_{rec} = 2(x,-x,-x,x)$. The shaped pulse on the ^{1}H channel is a one-lobe sinc pulse for restoring the water to the longitudinal magnetization. Pulsed field gradients (PFG) are used to suppress the water signal, artifacts and to select coherence transfer pathways with g1 and g2. SP1 and SP2 are a tanh/tan adiabatic half passage (AHP) and a time-reversed AHP. The duration of the AHP is 4 ms and the spin lock duration is t_{rel}. The positions a and b on the ^{1}H and ^{15}N channels indicate changes of the carrier frequencies. The ^{1}H carrier frequency is changed from the water chemical shift to the center of the amide proton chemical shift (8.2 ppm) at position a and is changed back to the water chemical shift at position b. The ^{15}N carrier frequency for AHP and spin-lock between a and b is different from that for the HSQC by Ω'. A ^{1}H continuous wave decoupling scheme was used during ^{15}N relaxation (t_{rel}) where the phase is alternated between x and −x every 10 ms ($4\tau_b$) (Korzhnev et al., 2002). The rf field strength of ^{1}H decoupling was 3.6 kHz at 8.2 ppm.

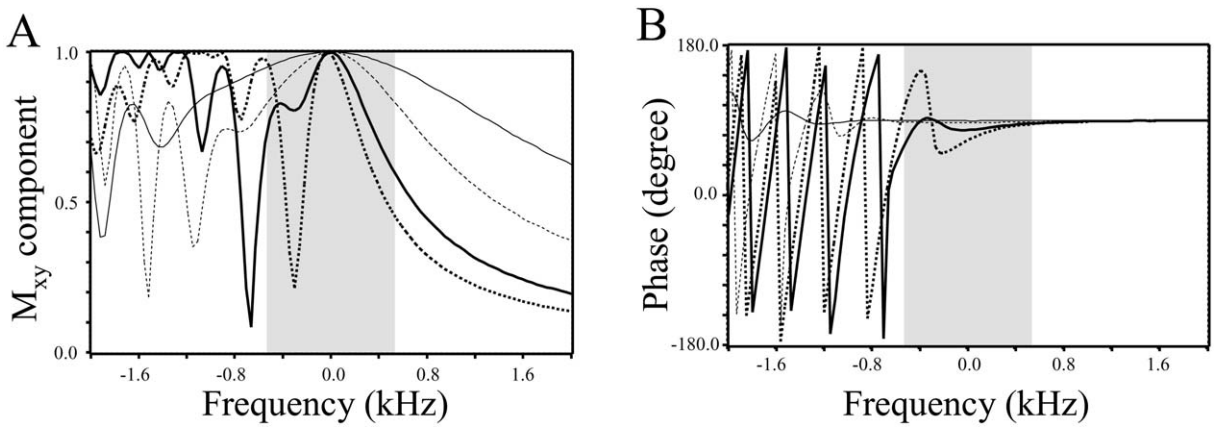

Figure 3. Excitation profiles of adiabatic half passage (AHP) pulses (Mulder et al., 1998; Garwood and Ke, 1991; Ugurbil et al., 1988). The amplitude and frequency modulated adiabatic pulse with a pulse length of 4 ms is defined by $\omega_1(t) = \omega_1^o \tanh(10t/\tau)$, $\Delta\omega(t) = \Delta\omega^o \tan(\text{atan}(50)(1\text{-}t/\tau))$ / 50 (Mulder et al., 1998). The pulse shape is presented in Figure S1 (Supplementary Materials). The simulated lines show the excitation profiles of the Mxy component (A) and the phase (B) as a function of rf field strength at 1600 (thin line), 800 (thin dotted line), 400 (thick line), and 275 (thick dotted line) Hz. The shaded regions show a spectral width of 1000 Hz corresponding to the ^{15}N spectral width. For uniform adiabatic rotations of ^{15}N magnetization by weak rf fields over a spectral width of 1000 Hz, relocating the carrier frequency or using a second AHP with reversed frequency modulation is required since the excitation profiles are not symmetric around the rf carrier position.

Pipe (Delaglio et al., 1995). The spectral widths were 5000 Hz and 1400 Hz for ^{1}H and ^{15}N respectively.

Results and discussion

The excitation profiles for the transverse magnetization (M_{xy}) and the phase rotation are simulated as a function of frequency for the tanh/tan adiabatic half passage pulses (AHP) (Mulder et al., 1998; Garwood and Ke, 1991; Ugurbil et al., 1988) (Figure 3). The simulations indicate that stronger fields show a wider excitation bandwidth for the transverse magnetization (Figure 3A) and a more uniform phase rotation (Figure 3B). The excitation profiles across all fields are

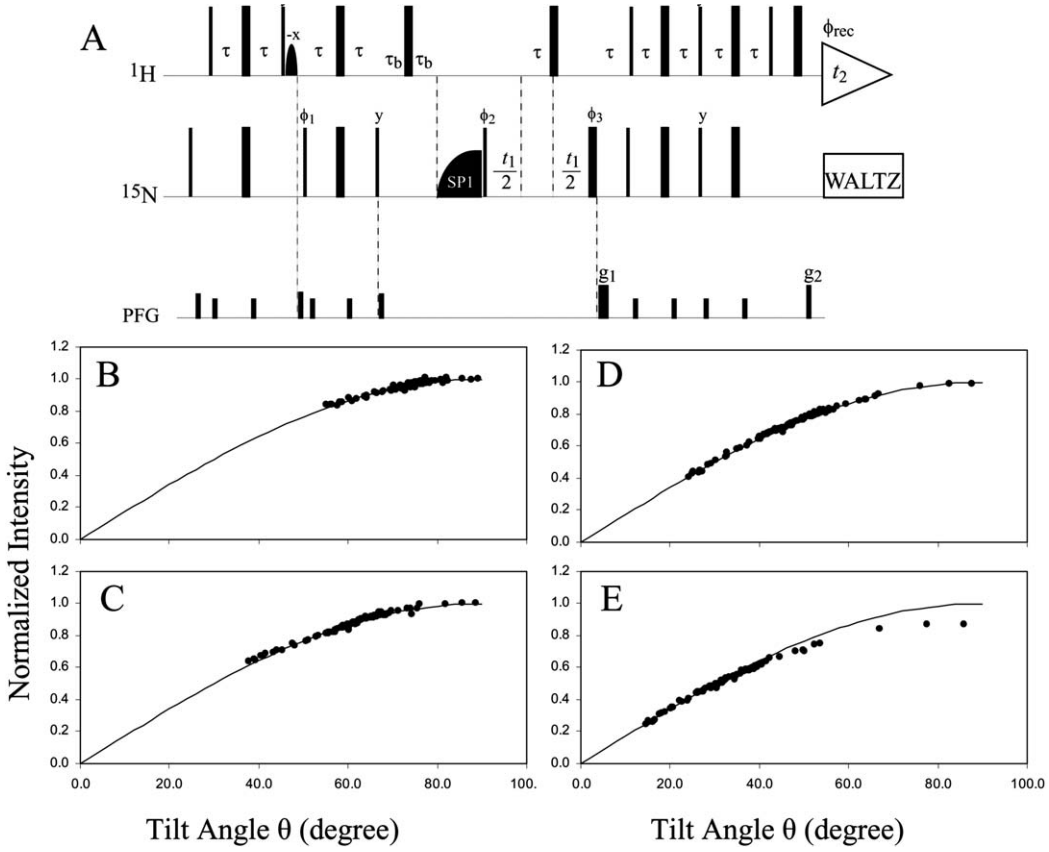

Figure 4. (A) Pulse sequence for measurement of M_x component of magnetization following adiabatic half passage (AHP) pulses at various field strengths. The AHP shaped pulse (SP1) and a 90° pulse with the phase ϕ_2 are inserted into a sensitivity-enhanced ^{1}H -^{15}N HSQC with refocused INEPT. Phase cycles are $\phi_1 = 8(x,-x)$; $\phi_2 = 4(x, x, -x,-x)$; $\phi_3 = 4(x),4(y),4(-x),4(-y)$; $\phi_{rec} = 2(x,-x, x, -x,-x, x, -x, x)$. The delays are the same as the pulse sequence in Figure 2. The ^{15}N carrier position is moved away from the center by 500 Hz to assure a large distribution of tilt angles over the HSQC spectral region. The power of the AHP shaped pulse is varied to achieve alignment of magnetization vectors of individual amides along different effective fields. Experimental normalized intensities of individual residues as a function of AHP power level versus tilt angle are plotted for $\omega_1 = 1510 \pm 38$ Hz (B), 816 ± 17 Hz (C), 471 ± 11 Hz (D), and 274 ± 9 Hz (E). The solid line represents the curve for perfect alignment of the magnetization represented by $M_x = M_b \sin\theta$. Experimentally, M_b values are obtained from the data at $\omega_1 = 1885 \pm 45$ Hz as sinθ values are close to 1.0. Peak intensities at lower ω_1 values are normalized against these M_b values. No phase correction was applied to the data in panels B, C, D and E.

not symmetric with respect to positive and negative frequency offset. Positive frequency offsets show uniformly decreasing M_{xy} magnetization as a function of offset whereas negative frequencies show oscillatory behavior for the magnetization. Similarly to the excitation profiles, the phase rotation profiles are not symmetric with respect to positive and negative frequency. Positive frequency offsets show an increase in the phase error as the field strength decreases. The consequence of the phase error, for example, for the on-resonance magnetization at 275 Hz is to reduce the x-component of the magnetization, Mx, to 0.9 as a result of a phase shift of 25°. When the rf field strength is greater than 1000 Hz and the carrier frequency is at the center of the ^{15}N spectral width, the magnetization is rotated to the xy-plane and the phase is essentially constant over the entire ^{15}N spectral width. However, at weaker rf fields, the magnetization can no longer be rotated across the entire ^{15}N spectral width due to the non uniform excitation profile at negative frequency offsets. In order to adiabatically rotate all the spins at weak fields, either a second AHP is used with a change in the sign of the frequency modulation or the frequency carrier position of the AHP is changed. The $R_{1\rho}$ experiment is performed by optimizing both the rf field strength and the rf carrier position so that tilt angles of 30° or greater are achieved for all magnetization within the ^{15}N spectral width. By sim-

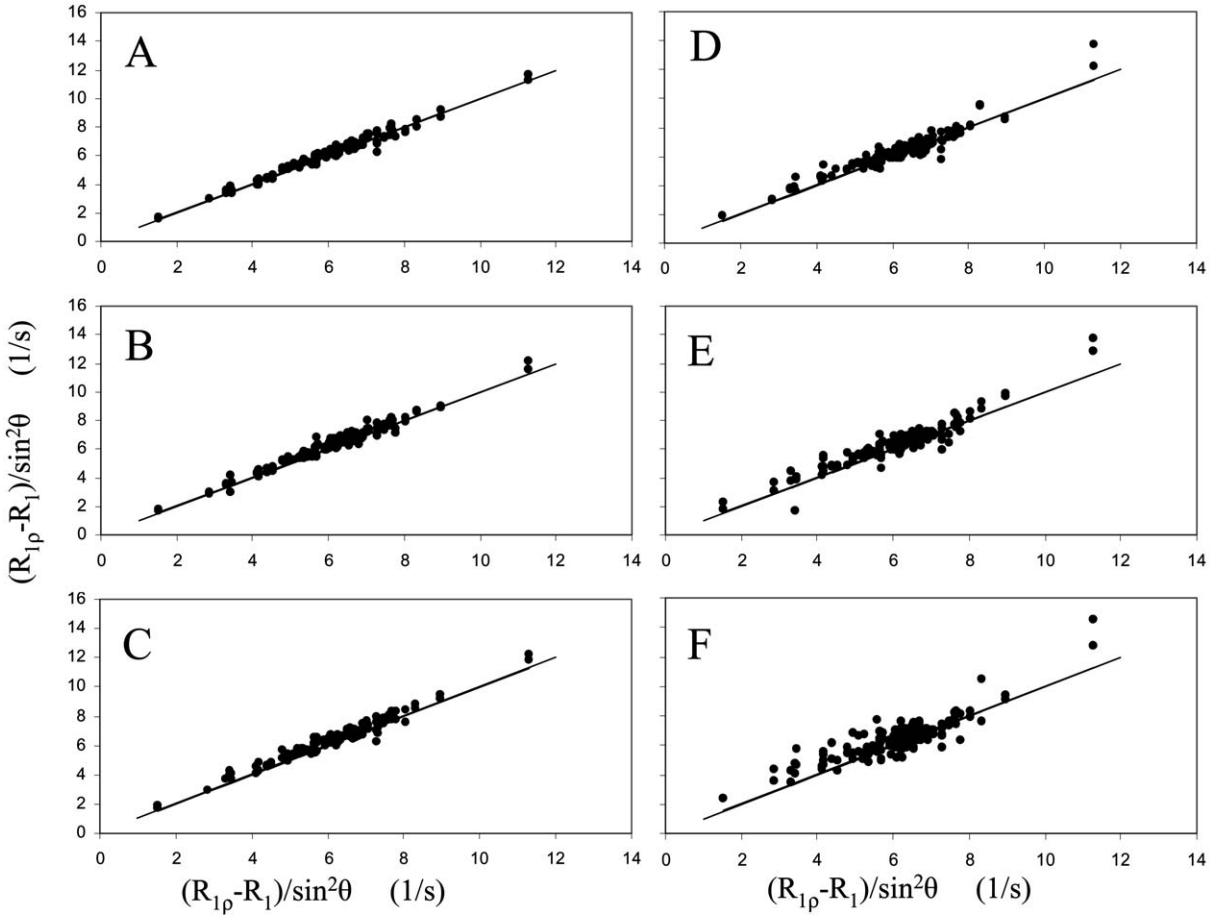

Figure 5. Comparison of $(R_{1\rho}\text{-}R_1)/\sin^2\theta$ values obtained from the pulse sequence of Figure 2 at different spin-lock field strengths. In all plots values of $(R_{1\rho}\text{-}R_1)/\sin^2\theta$ obtained with a spin-lock field strength of $\omega_1 = 1496 \pm 35$ Hz are plotted on the x-axis versus $(R_{1\rho}\text{-}R_1)/\sin^2\theta$ values with $\omega_1 = 1082 \pm 20$ (A), 785 ± 14 (B), 581 ± 12 (C), 440 ± 10 (D), 386 ± 9(E), and 275 ± 8 Hz (F) on the y-axis. Each plot has two sets of data points taken at $\Omega' = \pm 100$ (A), ± 200 (B), ± 300 (C), ± 400 (D), ± 500 (E), and ± 500 Hz (F). The averaged correlation coefficients are 0.99 (A), 0.98 (B), 0.95 (C), 0.98 (D), 0.94 (E), and 0.88 (F).

ultaneously varying both the experimental ω_1 field strength and the rf carrier frequency of the AHP during an experiment, each individual resonance experiences a range of tilt angles from 90° to approximately 30°. In conventional $R_{1\rho}$ experiments, the experiment is performed on resonance and the tilt angles range from 90° to 68° corresponding to a bandwidth of $\pm 0.4\omega_1$. In the experiments described herein, an asymmetric bandwidth from $+1.7\omega_1$ to $-0.5\omega_1$ is covered in a single experiment. A total bandwidth of $\pm 1.7\omega_1$ is obtained by performing the experiment a second time with a reversed adiabatic rotation thereby significantly increasing the range of accessible ^{15}N bandwidths.

To establish the degree of alignment of the individual resonances along the direction of the spin-lock field, particularly at weak fields, the intensity of the transverse magnetization resulting from the tanh/tan AHP is determined. The pulse sequence used to determine the M_x component of the magnetization following the AHP pulse at various field strengths consists of the AHP shaped pulse (SP1) inserted into a sensitivity-enhanced ^{1}H-^{15}N HSQC with refocused INEPT (Figure 4A). The delays are the same as those of the pulse sequence shown in Figure 2. The extent of alignment of the magnetization along the effective field is shown at multiple field strengths (Figures 4B–E) as a function of tilt angle θ. Perfect alignment is shown by the solid line which represents the theoretical intensity of the x-component of the magnetization arising from the adiabatic rotations as a function of tilt angle (see Figure 4 legend). Results indicate that for strong ω_1 the range of tilt angles is signific-

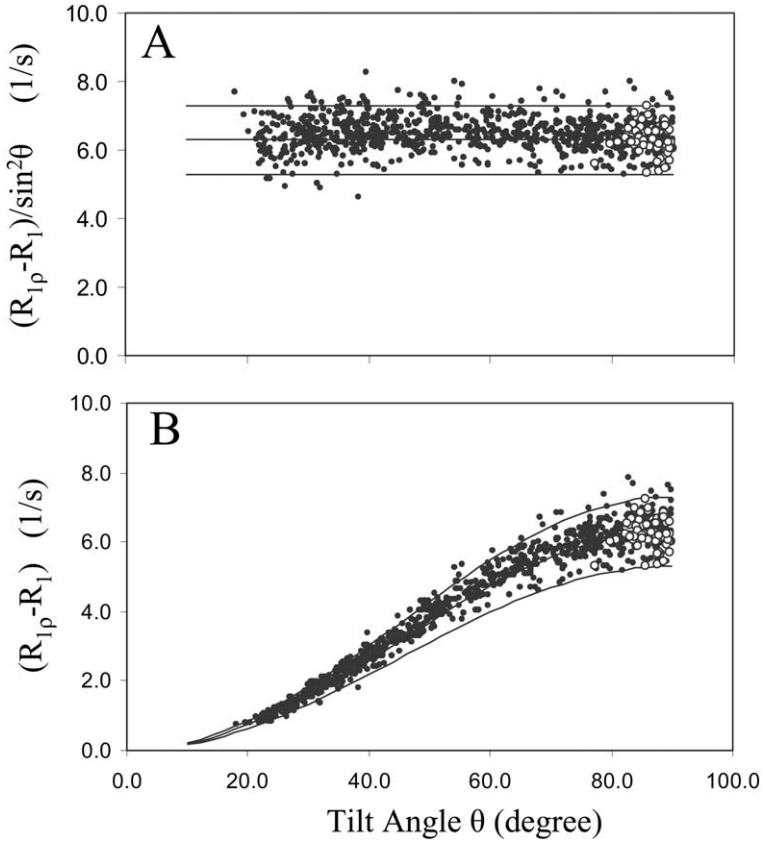

Figure 6. (A) $(R_{1\rho}\text{-}R_1)/\sin^2\theta$ values obtained from the $R_{1\rho}^{on/off}$ experiment in Figure 2 as a function of tilt angle θ. Open circles represent $(R_{1\rho}\text{-}R_1)/\sin^2\theta$ values at $\omega_1 = 1496$ Hz for 74 residues which were selected to be within ± 1.0 Hz deviation from the average $(R_{1\rho}\text{-}R_1)/\sin^2\theta$ value (6.3 Hz) shown in Figure 5. Closed circles are $(R_{1\rho}\text{-}R_1)/\sin^2\theta$ values for the same 74 residues with lower spin-lock field strengths of 1082, 785, 581, 440, 386, and 275 Hz. Solid lines at 5.3, 6.3, and 7.3 Hz are drawn to aid the eye and indicate that $(R_{1\rho}\text{-}R_1)/\sin^2\theta$ values are independent of tilt angle within this range. (B) $(R_{1\rho}\text{-}R_1)$ values as a function of tilt angle θ for the same 74 residues in shown in (A). Open circles are $(R_{1\rho}\text{-}R_1)$ values with $\omega_1 = 1496$ Hz and closed circles are $(R_{1\rho}\text{-}R_1)$ values obtained with lower spin lock field strengths of 1082, 785, 581, 440, 386, and 275 Hz. Three lines (5.3, 6.3, and 7.3 Hz at $\theta = 90°$) were drawn as a function of θ to aid the eye.

antly smaller than for weak fields and the intensity of the signal is higher. For field strengths ranging from 1499 Hz to 463 Hz the correlation between the experimental intensities and the theoretical intensities is excellent indicating that the adiabatic condition is achieved for all resonances. At weak fields of 275 Hz, the agreement between the theoretical intensities and the experimental data is excellent at small tilt angles, up to approximately 50°. For larger tilt angles, there is a small loss of intensity in the magnetization relative to the theoretical values. For example, at $\omega_1 = 274$ Hz (Figure 4E), the experimental $M_x = 0.87$ at a tilt angle of 86°. These data are consistent with the simulations shown in Figure 3 that indicate that at weak fields there is a phase rotation for residues that are close to resonance resulting in a small intensity loss to the x-component of the magnetization.

To evaluate the accuracy of the new pulse sequence, experimental results of the $R_{1\rho}^{on/off}$ experiment at strong field are compared both to a conventional R_2^{cpmg} experiment as well as to the new $R_{1\rho}^{on/off}$ experiment at multiple field strengths. Agreement between the $R_{1\rho}^{on/off}$ experiment at strong field ($\omega_1 = 1496$ Hz) and the R_2^{cpmg} experiment is excellent indicating that there are no systematic errors in the $R_{1\rho}^{on/off}$ experiment (Figure S3, Supplementary Material). The small deviation from a perfect correlation may come from slightly different effective field strengths in R_2^{cpmg} values versus $R_{1\rho}^{on/off}$ experiments. Comparison of the $R_{1\rho}^{on/off}$ experiment at a strong field with the exper-

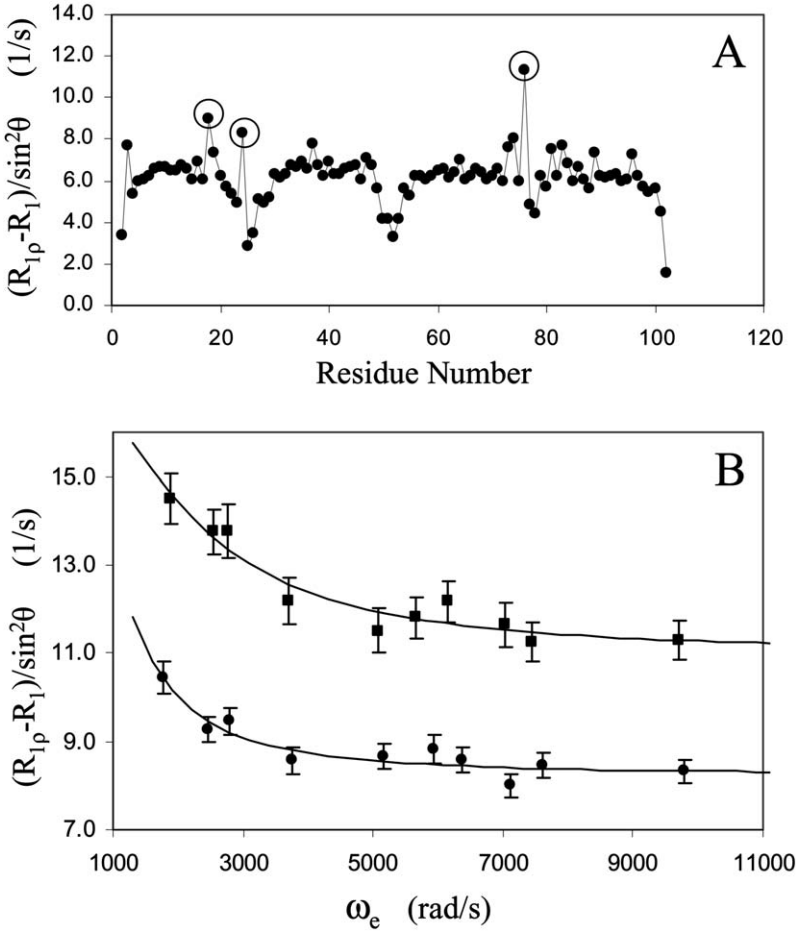

Figure 7. (A) $(R_{1\rho}-R_1)/\sin^2\theta$ values for the S-824 protein plotted as a function of residue. $R_{1\rho}-R_1$ data were obtained with ω_1 = 1496 Hz. $R_{1\rho}-R_1$ data were converted to $(R_{1\rho}-R_1)/\sin^2\theta$ by calculating θ from the ^{15}N chemical shifts of individual resonances and ω_1. The circled residues (N18, H24, and Q76) may have chemical exchange contributions to the $(R_{1\rho}-R_1)/\sin^2\theta$ data. (B) Relaxation dispersion for residues H24 (●) and Q76 (■) of the S-824 protein plotted as a function of ω_e. The relaxation dispersion data were fit with Equation 3 resulting in curves shown. For residue H24 at 126.24 ppm, 0.5($\delta\omega$), τ_{ex}, and R_2-R_1 were 105 ± 74.7 rad/s, 1.38 ± 2.66 ms, and 8.25 ± 0.17 1/s respectively. For residue Q76 at 125.13 ppm, 0.5($\delta\omega$), τ_{ex}, and R_2-R_1 were 117 ± 9.6 rad/s, 0.49 ± 0.29 ms, and 11.0 ± 0.43 1/s.

iment performed at weaker field strengths shows a good correlation overall (Figures 5A–F). Incorporation of recently developed decoupling schemes during the ^{15}N rotating frame relaxation period is critical to obtaining a good correlation between $R_{1\rho}^{on/off}$ at strong and weak fields (Korzhnev et al., 2002; Massi et al., 2004). From field strengths of 1082 to 386 Hz the correlation is greater than 0.94. At weak fields of $\omega_1 = 275$ Hz (Figure 5F), the correlation decreases to 0.88. The poorer correlation arises at extreme values of $(R_{1\rho}-R_1)/\sin^2\theta$. For large values of $(R_{1\rho}-R_1)/\sin^2\theta$, the correlation worsens as R_{ex} contributions become non negligible particularly at weak ω_1 values. For small values of $(R_{1\rho}-R_1)/\sin^2\theta$, the resonance offset correction term, $\sin^2\theta$, has a larger error propagation at weak ω_1 and low tilt angle θ.

In order to further examine the effect of weak fields or variable tilt angles on the performance of the pulse sequence shown in Figure 2, $(R_{1\rho}-R_1)/\sin^2\theta$ values of individual resonances were plotted as function of tilt angle (Figure 6A). A subset of resonances from Figures 5A–F corresponding to $(R_{1\rho}-R_1)/\sin^2\theta$ values of 6.3 ± 1.0 at $\omega_1 = 1496$ Hz were chosen for the plot of Figure 6A as these residues are thought to represent the overall molecular tumbling of the S-824 protein and do not have discernable R_{ex} contributions. $(R_{1\rho}-R_1)/\sin^2\theta$ values of the 74 selected residues are independent of tilt angle showing that the adiabatic

rotation of the magnetization provides effective alignment even at $\theta = 20°$. This result demonstrates the improvement of the $R_{1\rho}^{on/off}$ experiment when compared to conventional approaches which limits the tilt angles to higher than 68° for $R_{1\rho}^{on}$ experiments or lower than 50° for $R_{1\rho}^{off}$ experiments. In this experiment, $(R_{1\rho}\text{-}R_1)/\sin^2\theta$ values are obtained with a range of tilt angles from 90° to 30° to characterize R_{ex} contributions to $R_{1\rho}$.

To understand the contribution to experimental error, experimentally measured $(R_{1\rho}\text{-}R_1)$ values of the same 74 residues described above are plotted as a function of tilt angle (Figure 6B). Examples of relaxation decay curves for N18 and Q76, at 115.46 ppm and 125.13 ppm respectively, that are fit to obtain $(R_{1\rho}\text{-}R_1)$ values have similar line fitting errors to one another as a function of field strength for tilt angle (Figure S4, Supplementary Material). These data support the fact that the $(R_{1\rho}\text{-}R_1)$ values are not sensitive to resonance offset effects. As seen from the relaxation decay curves (Figure S4, Supplementary Material) and the plot of $(R_{1\rho}\text{-}R_1)$ versus tilt angle (Figure 6B), the values of $(R_{1\rho}\text{-}R_1)$ become smaller as the tilt angle gets smaller and the field strength gets weaker. For example, at $\theta = 90°$ the $(R_{1\rho}\text{-}R_1)$ values are 6.3 ± 1.0 1/s on average, whereas at $\theta = 30°$ the values are reduced to 1.58 ± 0.25 1/s. In the analysis of the experiments, a resonance offset correction is required and the data are converted from $(R_{1\rho}\text{-}R_1)$ to $(R_{1\rho}\text{-}R_1)/\sin^2\theta$; for example, when $(R_{1\rho}\text{-}R_1)$ rates at $\theta = 30°$ are converted to $(R_{1\rho}\text{-}R_1)/\sin^2\theta$ values, a factor of 4 is multiplied to both the rates and the errors. Therefore the percent error in the resonance offset corrected data is higher at low tilt angles and weak fields. These errors at low tilt angle and weak field in the resonance offset corrected data can explain the poorer correlation seen for small values of $(R_{1\rho}\text{-}R_1)/\sin^2\theta$ in the plot of Figure 5F with $\omega_1 = 275$ Hz. In light of these errors, for the experiments described here the minimum rf field strength that was used was 275 Hz and the corresponding minimum effective field strength for each resonance was in the range of 1750–3500 rad/s. The advantage to the approach described herein is that for each individual resonance, a wide range of tilt angles (from 30° to 90°) is used thereby reducing systematic error in the experiment.

The $(R_{1\rho}\text{-}R_1)/\sin^2\theta$ relaxation rates of 101 resonances are plotted for the four helix bundle protein S-824 (Figure 7A). The overall structure of the protein is in up-down-up-down four helix bundle where helices span residues 5–20 (helix 1), 28–48 (helix 2), 56–72 (helix 3), and 80–99 (helix 4) (Wei et al., 2003a, 2003b). Examination of Figure 7A indicates that residues N18 at the C-terminal end of helix 1, H24 at the loop region between helix 1 and 2, and Q76 at the loop region between helix 3 and 4 have relatively large $(R_{1\rho}\text{-}R_1)/\sin^2\theta$ values at $\omega_1 = 1496$ Hz implying that R_{ex} may be contributing to $R_{1\rho}$ for these residues. With the exception of the loop regions which show relatively small $(R_{1\rho}\text{-}R_1)/\sin^2\theta$ values, the remaining residues do not appear to have many deviations from the average value. In Figure 7B, $(R_{1\rho}\text{-}R_1)/\sin^2\theta$ values of residues H24 and Q76 are plotted as function of ω_e which is calculated from the combined array of (ω_1, Ω') and the chemical shift of each resonance in the HSQC. N18 did not show measurable relaxation dispersion up to the minimum $\omega_e = 3027$ rad/s that is experimentally attained for this residue. This may be due to exchange time scales that are either faster or slower than the window of the observable timescale resulting from these experiments. The data for H24 and Q76 were fit to Equation 3 with three parameters, $R_2\text{-}R_1$, $P_A P_B(\delta\omega)^2$, and τ_{ex} using the Marquard algorithm (Press et al., 1992).

$$(R_{1\rho} - R_1)/\sin^2\theta = (R_2 - R_1) + P_A P_B(\delta\omega)^2\tau_{ex}/(1 + \tau_{ex}^2\omega_e^2). \quad (3)$$

The data show that the exchange rates for H24 (1.38 ± 2.66 ms) and Q76 (0.49 ± 0.29 ms) are in the millisecond timescale regime suggesting some restricted motion between loops. In examining the structure it is interesting to note that these two loops are on the same side of the three dimensional structure (Wei et al., 2003b).

In summary, the $R_{1\rho}^{on/off}$ experiment described here allows the measurement of dynamics on the order of 0.05 to 1.0 ms across a broad range of ^{15}N frequencies. Access to these timescales, along with those measured from $R_{1\rho}^{off}$ and R_2 CPMG-type experiments provides the opportunity to investigate conformational fluctuations of macromolecules over two orders of magnitude.

Acknowledgements

This work is supported by NIH grant GM45302 to J.B. We thank Prof M.H. Hecht and Dr Y. Wei for providing the S-824 protein sample.

Supporting Information Available: Four figures (Figure S1–S4) at http://kluweronline.com/issm/0925-2738.

References

Akke, M. and Palmer III, A.G. (1996) *J. Am. Chem. Soc.*, **118**, 911–912.

Akke, M., Liu, J., Cavanagh, J., Erickson, H.P., and Palmer III, A.G. (1998) *Nat. Struct. Biol.*, **5**, 55–59.

Bax, A., Ikura, M., Kay, L.E., Torchia, D.A., and Tschudin, R. (1990) *J. Magn. Reson.*, **86**, 304–318.

Carver, J.P. and Richards, R.E. (1972) *J. Magn. Reson.*, **6**, 89–105.

Davis, D.G., Perlman, M.E., and London, R.E. (1994) *J. Magn. Reson. B*, **104**, 266–275.

Delaglio, F., Grzesiek, S., Vuister, G.W., Zhu, G., Pfeifer, J., and Bax, A. (1995) *J. Biomol. NMR*, **6**, 277–293.

Deverell, C., Morgan, R.E., and Strange, J.H. (1970) *Mol. Phys.*, **18**, 553–559.

Frauenfelder, H., Sligar, S.G., and Wolynes, P.G. (1991) *Science*, **254**, 1598–603.

Garwood, M. and Ke, Y. (1991) *J. Magn. Reson.*, **94**, 511–525.

Guenneugues, M., Berthault, P., and Desvaux, H. (1999) *J. Magn. Reson.*, **136**, 118–126.

Kay, L.E. (1998) *Nat. Struct. Biol.*, **5**, 513–517.

Korzhnev, D.M., Skrynnikov, N.R., Millet, O., Torchia, D.A., and Kay, L.E. (2002) *J. Am. Chem. Soc.*, **124**, 10743–10753.

Loria, J.P., Rance, M., and Palmer III, A.G.P. (1999) *J. Am. Chem. Soc.*, **121**, 2331–2332.

Massi, F., Johnson, E., Wang, C., Rance, M., and Palmer III, A.G. (2004) *J. Am. Chem. Soc.*, **126**, 2247–2256.

Mulder, F.A.A., de Graaf, R.A., Kaptein, R., and Boelens, R. (1998) *J. Magn, Reson.*, **131**, 351–357.

Mulder, F.A.A., van Tilborg, P.J.A., Kaptein, R., and Boelens, R. (1999) *J. Biomol. NMR*, **13**, 275–288.

Orekhov, V.Y., Pervushin, K.V., and Arseniev, A.S. (1994) *Eur. J. Biochem.*, **219**, 887–896.

Palmer III, A.G. (1997) *Curr. Opin. Struc. Biol.*, **7**, 732–737.

Palmer III, A.G., Williams, J., and McDermott, A. (1996) *J. Phys. Chem.*, **100**, 13293–13310.

Palmer III, A.G., Kroenke, C.D., and Loria, J.P. (2001) *Meth. Enzymol.*, **339**, 204–238.

Press, W.H., Teukolsky, S.A., Vetterling, W.T., and Flannery, B.P. (1992) *Numerical Recipies in C*, 2nd edn., Cambridge University Press, New York, NY.

Szyperski, T., Luginbühl, P., Otting, G., Güntert, P., and Wüthrich, K. (1993) *J. Biomol. NMR*, **3**, 151–164.

Trott, O. and Palmer III, A.G. (2002) *J. Magn. Reson.*, **154**, 157–160.

Ugurbil, K., Garwood, M., Rath, A. R., and Bendall, M. R. (1988) *J. Magn. Reson.*, **78**, 472–497.

Wang, C., Grey, M. J., and Palmer III, A. G. P. (2001) *J. Biomol. NMR*, **21**, 361–366.

Wei, Y., Fela, D., Kim, S., Hecht, M.H., and Baum, J. (2003a) *J. Biomol. NMR*, **27**, 395–396.

Wei, Y., Kim, S., Fela, D., Baum, J., and Hecht, M.H. (2003b) *PNAS*, **100**, 13270–13273.

Zinn-Justin, S., Berthault, P., Guenneugues, M., and Desvaux, H. (1997) *J. Biomol. NMR*, **10**, 363–372.